Eur. Phys. J. E **28**, 165–171 (2009)
DOI 10.1140/epje/i2008-10387-2

THE EUROPEAN PHYSICAL JOURNAL E

Regular Article

Temperature-sensitive poly(N-Isopropyl-Acrylamide) microgel particles: A light scattering study

M. Reufer[1,2], P. Díaz-Leyva[1], I. Lynch[3], and F. Scheffold[1,a]

[1] Department of Physics and Fribourg Center for Nanomaterials, University of Fribourg, CH-1700 Fribourg, Switzerland
[2] Adolphe Merkle Institute, University of Fribourg, CH-1700 Fribourg, Switzerland
[3] School of Chemistry and Chemical Biology, University College Dublin, Belfield, Dublin 4, Ireland

Received 11 August 2008
Published online: 25 November 2008 –

Abstract. We present a light scattering study of aqueous suspensions of microgel particles consisting of poly(N-Isopropyl-Acrylamide) cross-linked gels. The solvent quality for the particles depends on temperature and thus allows tuning of the particle size. The particle synthesis parameters are chosen such that the resulting high surface charge of the particles prevents aggregation even in the maximally collapsed state. We present results on static and dynamic light scattering (SLS/DLS) for a highly diluted sample and for diffuse optical transmission on a more concentrated system. In the maximally collapsed state the scattering properties are well described by Mie theory for homogenous hard spheres. Upon swelling we find that a radially inhomogeneous density profile develops.

PACS. 82.70.Dd Colloids – 83.80.Kn Physical gels and microgels – 82.70.Gg Gels and sols

1 Introduction

Colloidal particles with adjustable interaction potential have been of scientific and technological interest in recent years due to their potential use to control bulk properties such as viscous flow, optical and also magnetic properties [1–7]. Thermo-sensitive microgels have been widely used as model systems [2,8–10]. These materials have also received attention due to their potential applications in drug delivery or as sensors as a result of their "responsive" characteristics following changes in their environment [11]. One of the most widely studied systems is *poly(N-Isopropyl-Acrylamide)* (PNIPAM), a polymer which has a critical solution temperature of approximately 33 °C. PNIPAM colloids can be prepared by cross-linking PNIPAM resulting in microgel particles with tunable softness (and swelling degree), these depending on the cross-link density. Another approach is to coat well-defined solid core particles with PNIPAM, thereby exploiting properties of both materials [8].

Both pure PNIPAM and PNIPAM-coated particles display properties due to the tunable network combined with properties of classical colloids, *e.g.* crystallization or aggregation. This is very useful to tailor colloidal systems that can be kept close to the liquid-solid transition, thus having the possibility to "temper" these materials [12]. Tempering is not possible using most "classical" colloidal systems that require a change in composition in order to cross a phase boundary. In this respect temperature-sensitive particles are ideal candidates to provide quantitative information about the ergodic–nonergodic-transition in systems with repulsive interactions, both for the glass transition [13–17] as well as for crystallization [18].

At temperatures well above 35 °C the PNIPAM particles are collapsed and behave as solid spheres. The effective interaction potential can be either attractive due to van der Waals forces which lead to aggregation and phase separation [19], or, in the presence of surface charges, the particles can be stabilized in suspension. Upon lowering the temperature the particles swell by a factor of two to five in size [2,20]. If the initial particle density is sufficiently high, the particle volume increase can drive the system from a liquid to a solid state. A number of rheological studies were able to study in detail the apparent divergence of the viscosity at the transition point and the emergence of an elastic shear modulus [2,21]. More recently, studies on the internal dynamics and the frequency- and shear-rate-dependent rheology close to and above the liquid-solid transition have been reported [22,23].

In this article we discuss the temperature-dependent properties of highly cross-linked microgel particles. The focus of the present work is on a comprehensive optical characterization of PNIPAM microgel suspensions. We present results on static and dynamic light scattering (SLS/DLS) for a highly diluted sample and for diffuse optical transmission on a more concentrated system.

[a] e-mail: Frank.Scheffold@unifr.ch

A detailed understanding of the temperature-dependent structural properties of individual particles is a key ingredient for the study of the dynamic properties and the phase behavior of dense suspensions. The parameters of the synthesis were chosen such that the effective surface charge prevents aggregation even in the maximally collapsed state. The advantage of such a charge-stabilized system is that the equilibrium (or quasi-equilibrium) properties can be studied over the whole range of temperatures even at high volume fraction. In the current article we discuss the structural aspects of our PNIPAM suspension. A detailed study of the high-density phase behaviour and rheological properties will be presented elsewhere [22].

The outline of this article is as follows: In Section 2 we describe the particle chemistry and the particle characterization by scanning electron microscopy. In Section 3 we analyze the temperature dependence of the hydrodynamic radius and in Section 4 we discuss results from static light scattering on a dilute suspension. In Section 5 we study the optical properties (diffuse transmission) of a concentrated suspension. Finally, in Section 6 the experimental results are summarized.

2 Sample preparation

We use free radical cross-linking polymerization of the monomer *N-Isopropyl-Acrylamide* (NIPAM) from Acros Organics (Acros Organics BVBA, Geel, Belgium) with the tetra-functional cross-linker *N,N′-Methylene-Bis-Acrylamide* (BIS) from Fluka (Fluka Chemie GmbH, Buchs, Switzerland). The BIS molecules are essentially two acrylamide monomer units bridged by a covalent bond [24]. The polymerization reaction is initiated using the ionic salt *Potassium Persulfate* (KPS, Merck KGaA, Darmstadt, Germany). All chemicals are reagent grade and used without further purification, except NIPAM which is recrystallized from N-Hexane solution. The synthesis is performed by dissolving a mixture of monomer NIPAM and cross-linker BIS (at 21.43 mg/ml) in 145 ml deionized and filtered water[1] . The cross-linking ratio, defined by $f_{\rm bis} \equiv [\rm BIS]/([\rm NIPAM] + [\rm BIS])$ is 6.7%. Such a relatively high ratio is expected to produce a rigid gel with approximately one molecule of cross-linker per 19 molecules of monomer [20,25,26]. The mixture (previously degassed for $\sim$ 30 minutes) is heated up to 80 °C under pure nitrogen atmosphere. Then, 72.8 mg of KPS dissolved in 5 ml of degassed water is added to the mixture to start the polymerization reaction. The reaction proceeds for at least 4 hours at constant temperature. Finally the dilute suspension is extensively dialyzed for several days against deionized water to eliminate unreacted monomer excess [8,27,28]. The final step is carried out under normal atmospheric conditions which leads to a finite solvent ionic strength due to spontaneous dissolution of carbon dioxide in water. Dense suspensions are prepared using a rotary evaporator. This procedure increases both the particle density as well as the ionic strength of the solvent. In turn, at high temperatures, we expect to obtain a charge-stabilized suspension with a strongly screened Coulomb interaction potential. We do not observe any aggregation at high temperatures which indicates that the suspension is stable.

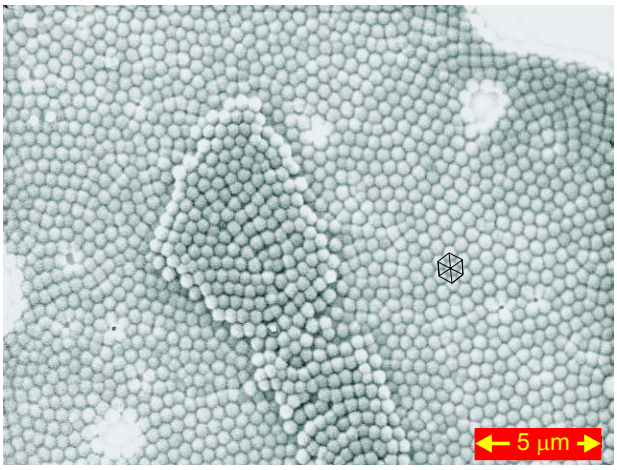

Fig. 1. Scanning electron microscopy picture of PNIPAM particles in the collapsed state (particle radius 260 ± 5 nm).

Figure 1 shows a scanning electron micrograph of our PNIPAM particles on a solid substrate. The particles are ordered in hexagonal arrays, giving us a qualitative idea about the rather low polydispersity in the collapsed state. From the analysis of several dozen particle positions, we obtain a SEM radius of 260 ± 5 nm.

It is well known that even in the maximally collapsed state PNIPAM microgel particles contain a non-negligible amount of water molecules. The presence of this *bound water* has to be taken into account for the characterization of PNIPAM colloidal suspensions. As shown by Lele *et al.* [29] the bound water content of a collapsed PNIPAM gel is approximately 0.38–0.4 gram per gram of polymer which corresponds to a bound water volume fraction of approximately $\Phi_{\rm Water} = 30\%$ if we assume a water density of 1 g/cm^3 and a bulk density of PNIPAM approximately 1.1 g/cm^3 [2,30,31].

As suggested by Erbe *et al.* [32] the bulk refractive index of PNIPAM for visible light can be estimated by extrapolating literature dn/dc values [33]. One finds $n = 1.52 \pm 0.01$. We note that similar chemical structures such as Poly(N-butylmethacrylamide), Poly(N-2-methoxyethyl) methacrylamide, Poly(N-methylacrylamide) all have bulk indices for visible light in the range 1.51–1.54 [34]. If we assume a value of 1.33 for the refractive index of bound water, we can estimate the refractive index of the particles in the maximally collapsed state based on the Maxwell-Garnett mixing rule [35,36]. For the case of small refractive index variations it can be written as: $n \simeq \Phi_{\rm Water} \cdot 1.33 + \Phi_{\rm Polymer} \cdot 1.52 = 1.46$.

[1] The original batch further contained a small quantity of TiO_2 nanoparticles in an initial attempt to create core shell particles. From transmission electron microscopy we find no trace of the TiO_2 in sample after concentration and purification. Therefore the system under study consists exclusively of PNIPAM particles suspended in water.

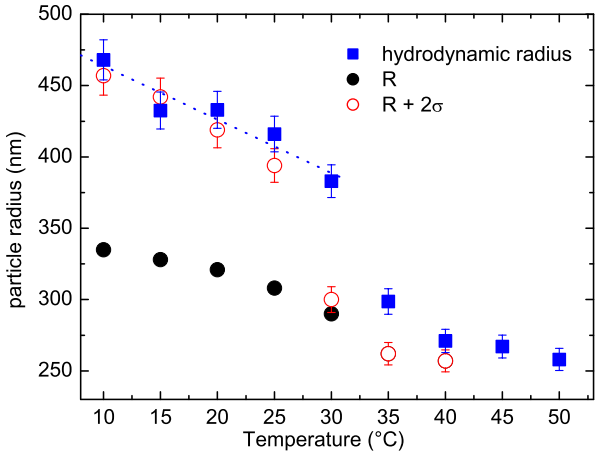

Fig. 2. Size characterization by dynamic light scattering (DLS). Full squares: temperature-dependent hydrodynamic radius $R_{\rm H}$ (error bars denote spread of data points for measurements at three different angles $\theta = 60°, 40°, 20°$) at $\Phi \sim 10^{-5}$. Full circles: mean radius of mass distribution R. Open circles: mean radius R plus diffuse layer 2σ.

3 Hydrodynamic radius from dynamic light scattering

We determine the hydrodynamic radius of the particles using standard dynamic light scattering in the single scattering regime with $\lambda = 532\,\text{nm}$ (goniometer system ALV/SP-125, ALV, Germany). A low volume fraction ($\Phi \sim 10^{-5}$) the colloidal suspension is filled into a cylindrical glass tube of 10 mm inner diameter. The vial is placed in the center of a cylindrical vat filled with an index-matching fluid, cis-trans decahydronaphthalene (decalin), in order to reduce stray light reflections and scattering from the vial surface. The index-matching fluid is temperature controlled ($\pm 0.1\,°\text{C}$).

From the measured time-averaged intensity correlation function, $g^{(2)}(q,\tau)$ the translational free diffusion is determined and the particle hydrodynamic radius extracted by common procedures [37,38]. We restrict the analysis to relatively low scattering angles ($\theta = 60°, 40°, 20°$). The experimental data, Figure 2, shows the expected strong temperature dependence. Since PNIPAM is not soluble in hot water ($T > 33°$) the cross-linked PNIPAM gels collapse at elevated temperatures, whereas at room temperature and below water is a good solvent leading to a strong swelling. As a consequence of the relatively high cross-link density, the swelling is less pronounced compared to some of the previous studies where swelling ratios up to four or five have been reported [20,25,26].

4 Static light scattering

We determine the particle form factor over a temperature range $15\,°\text{C} \leq T \leq 40\,°\text{C}$ using a home-built *3D Light Scattering* setup [39]. We use a solid-state laser TUI Optics DL 100R (TUI Optics GmbH, Munich, Germany) $\lambda = 680.4\,\text{nm}$, two avalanche photomultipliers Perkin Elmer SPCM-AQR-13-FC (Perkin Elmer Inc, Fremont CA, U.S.A.) and a digital multi-tau correlator (Correlator.com, Bridgewater NJ, U.S.A.). The sample is contained in a cylindrical optical glass tube of 5 mm inner diameter, placed in the center of a vat filled with cis/trans decalin to reduce stray light contributions.

The q dependence of the scattering intensity $I(q) \propto P(q)$ of a dilute sample ($\Phi \approx 4 \times 10^{-5}$) is displayed in Figure 3 for different temperatures. For uncorrelated spherical particles $I(q)$ is given by the scattering form factor $P(q) = k_0^2 \frac{\mathrm{d}\sigma_{\rm sc}}{\mathrm{d}\Omega}$, where $k_0 = 2\pi n_s/\lambda$ [40]. In the high-temperature limit the experimental data can be described by a Mie calculation for a homogenous sphere of diameter 242 nm, refractive index $n = 1.46$ and a polydispersity of 9% [41].

The SLS particle size in the maximally collapsed state $R = 242\,\text{nm}$ is found in rather good agreement with the hydrodynamic radius $R_{\rm H} \simeq 260\,\text{nm}$. The result is also consistent with the SEM analysis although, if under vacuum conditions all the water is released, we would actually expect to find a radius of about 215 nm. There are a number of possible reasons for this slight difference. For example we cannot exclude the possibility that some residual water remains bound to the polymer or that the particles are slightly deformed leading to a flattened shape [20]. Small errors in the alignment of the electron microscope or the calibration could also explain this difference. More experiments would be needed to provide a conclusive answer, which is beyond the scope of this work.

Lowering the temperature the first minimum is expected to shift to lower q values due to the increasing particle size [42,26]. Such a variation is indeed observed. A quantitative description of the data, however, requires modeling of the density profile in the particle.

Stieger and coworkers [26] suggested a convolution of the density profile for a particle of radius R with a Gaussian of width σ, implying an effective steric radius of order $R_{\rm H} \approx R + 2\sigma$. An alternative approach suggested by Mason and Lin is the "uniform core linear shell" [43]. Both models provide an excellent fit to the data for temperatures of $T = 25\,°\text{C}$ and below where the particles are swollen and the effective refractive index is sufficiently low for the Rayleigh-Gans-Debye (RGD) approximation ($|n/n_{\rm solvent} - 1| \ll 1$) to be valid. The "uniform core linear shell" model, however, results in an outer cut-off radius substantially smaller than the hydrodynamic radius (data not shown). For this reason we have chosen to apply the Gaussian approximation. We think that the latter model captures better the slow and gradual decrease of the particle density in the particle corona. One should keep in mind however, as pointed out by Mason and Lin, that the missing cut-off makes this model unphysical at very large radial distances.

Both the "uniform core linear shell" and the Gaussian approximation were originally applied to neutron scattering data. In the RGD limit light and small-angle neutron scattering on a two-component system are sensitive

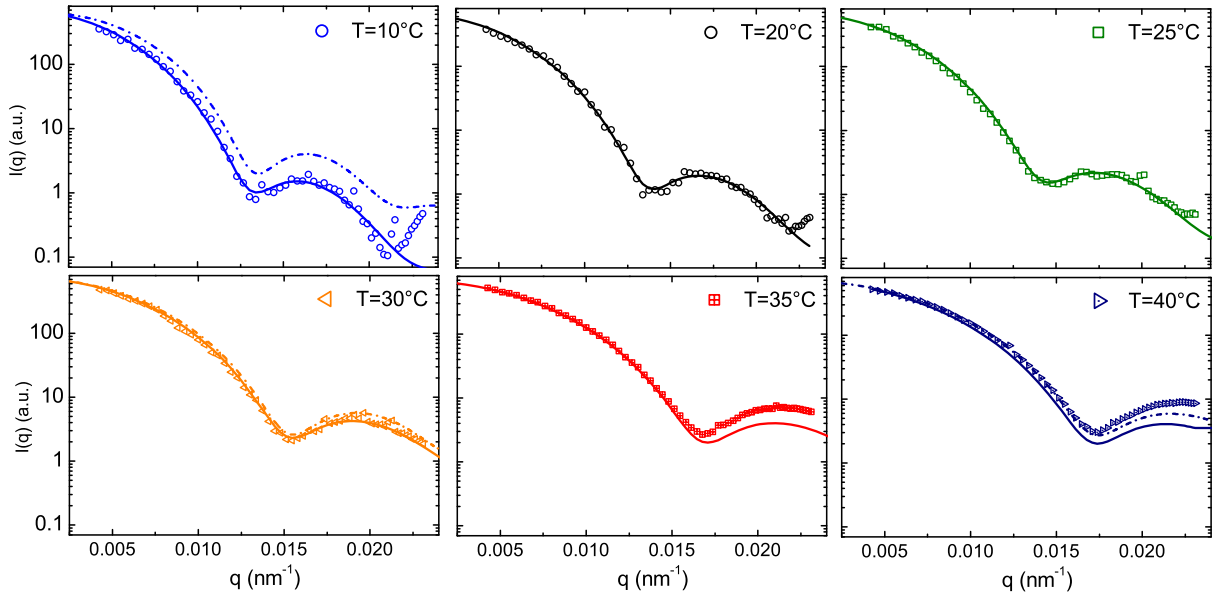

Fig. 3. Temperature-dependent form factor $P(q)$ measured under dilute conditions ($\Phi \approx 4 \times 10^{-5}$). Dash-dotted lines: Mie calculations for homogenous spheres, polydispersity 9%: ($R_{\mathrm{Mie}} = 242\,\mathrm{nm}$, $n = 1.46$, $T = 40\,^{\circ}\mathrm{C}$), ($R_{\mathrm{Mie}} = 275\,\mathrm{nm}$, $n = 1.42$, $T = 30\,^{\circ}\mathrm{C}$) and ($R_{\mathrm{Mie}} = 350\,\mathrm{nm}$, $n = 1.37$, $T = 10\,^{\circ}\mathrm{C}$). Solid lines: RGD form factor for a mass distribution with mean radius R convoluted with a Gaussian with standard deviation σ, polydispersity $9.5 \pm 0.5\%$.

Table 1. Hydrodynamic radius R_{H} and static light scattering parameter from a best fit to a RGD form factor assuming a gradually decreasing density profile with a mean radius R convoluted with a Gaussian of width σ.

$T(^{\circ}\mathrm{C})$	R_{H}	R	σ
10	468	335	61
15	433	328	57
20	433	321	49
25	416	308	43
30	383	290	5
35	299	262	0
40	271	257	0
45	267		
50	258		

to the same physical properties, namely density fluctuations. Light scattering probes fluctuations of the refractive index $(n/n_{\mathrm{solvent}} - 1)$, whereas neutron scattering probes fluctuations in the nuclear scattering length density. Both quantities are proportional to the local polymer density. Therefore, up to a prefactor, the model by Stieger and coworkers [26] can be applied to both light and neutron scattering data. In the RGD approximation the scattering form factor is given by $P(q) \propto [A(q)]^2$, with

$$A(q) = 3\exp[-(\sigma q)^2/2][\sin(qR) - qR\cos(qR)]/(qR)^3. \quad (1)$$

It is straightforward to account for polydispersity using standard procedures [38] (polydispersity values for best fit to the data are $9.5 \pm 0.5\%$). We obtain an excellent fit to the data for temperatures up to $T = 30\,^{\circ}\mathrm{C}$. $T = 30\,^{\circ}\mathrm{C}$ is, however, a borderline case. Here, we obtain a perfect RGD fit with $\sigma \approx 0$, while a Mie calculation with the same parameters displays differences. This inconsistency shows that the RGD condition ($|n/n_{\mathrm{solvent}} - 1| \ll 1$) is not fully met. As a consequence, in this transition regime, the thickness of the diffuse corona σ is underestimated.

Figure 2 and Table 1 summarize the results of our analysis. For temperatures $T = 25\,^{\circ}\mathrm{C}$ and below the results from static (open circles) and dynamic light scattering (solid squares) match almost perfectly. However in the transition regime at $T = 30\,^{\circ}\mathrm{C}$ we observe a noticeable difference.

It is worthwhile to add that our study represents one of the first attempts to quantitatively model the full form factor (including the first minimum) of PNIPAM particles using static light scattering. Our results clearly show that such data can be of similar or even better quality than neutron scattering data but with significantly less sample preparation requirements and at a fraction of the cost. This should prove very useful for future studies of these very interesting systems in particular for particle radii of about 200 nm and above. A detailed understanding of the rheological properties in the solid state for example will require quantitative input concerning the internal polymer density distribution.

5 Diffusing transmission

The optical transmission through a cell of thickness L is determined by the scattering cross-section of the individual particles, the particle number density and interparticle correlations characterized by the structure factor $S(q)$. For dilute non-interacting systems ($S(q) \equiv 1$) the

optical properties can be characterized by the scattering mean free path [44]

$$l = \frac{1}{\rho \frac{2\pi}{k_0^2} \int_0^{2k_0} P(q)\, q\, \mathrm{d}q} = \frac{1}{\rho \sigma_{\mathrm{sc}}}, \tag{2}$$

which is found to be inversely proportional to the total scattering cross-section of a particle σ_{sc}. Initially this leads to an exponential decay of the unscattered intensity transmitted through a slab of thickness L: $T_0 = \exp(-L/l)$. With increasing density multiple scattering contributions become important until in the case of a highly turbid system light propagates diffusively and the total transmission coefficient can be written as [44]

$$T \propto l^*, \qquad L \gg l^*. \tag{3}$$

The typical length characterizing the diffusion process is the transport mean free path l^* which can be written quite generally in terms of the mean-square scattering vector [45]

$$\frac{l^*}{l} = \frac{2\, k_0^2}{\langle\, q^2 \,\rangle}, \tag{4}$$

$\langle\ \rangle$ denotes the angular average over all scattering angles, weighted by the scattering probability.

Positional correlations between particles affect the optical density of concentrated colloidal suspensions because they change the angular distribution of scattered light emerging from each scattering event and therefore change the value of l^*. For correlated systems we replace $P(q)$ by the full scattering function $P(q)\, S(q)$, thus we obtain

$$\langle\, q^2 \,\rangle = \frac{1}{k_0^2} \frac{\int_0^{2k_0} P(q)\, S(q)\, q^3\, \mathrm{d}q}{\int_0^{2k_0} P(q)\, S(q)\, q\, \mathrm{d}q}. \tag{5}$$

Therefore the general expression for l^* in a correlated suspensions of spherical particles reads [45,46]

$$l^* = k_0^6 \left(\pi\, \rho \int_0^{2k_0} P(q)\, S(q)\, q^3\, \mathrm{d}q \right)^{-1}. \tag{6}$$

We now want compare these predictions to the scattering properties of our thermosenstive PNIPAM particles. A dense suspension is prepared using a rotary evaporator from the initial as-synthesized stock solution. From drying and weighing we find a mass density of $\approx 14.6\%$ w/w. Under the assumption that the dry sample is absolutely water free, this would imply a volume fraction in the collapsed state of $\Phi \approx 19\%$. We perform a diffuse transmission experiment with a frequency-doubled Nd:YV_{04} solid-state laser Coherent "Verdi" (Coherent Inc., Santa Clara CA, U.S.A.) operating at $\lambda = 532\,\mathrm{nm}$. The laser beam is slightly expanded to illuminate the sample with a spot size diameter of approximately 5 mm. The sample is kept in a regular glass cell with inner dimensions $10 \times 2\,\mathrm{mm}$ (Hellma, Germany). The scattered light leaving the sample is collected by a single-mode optical fiber placed in transmission geometry. The transport mean free path l^* at each temperature is obtained by measuring the ratio of the intensity of the transmitted light through the sample compared to the value obtained for a reference sample of known value l^* [47,48].

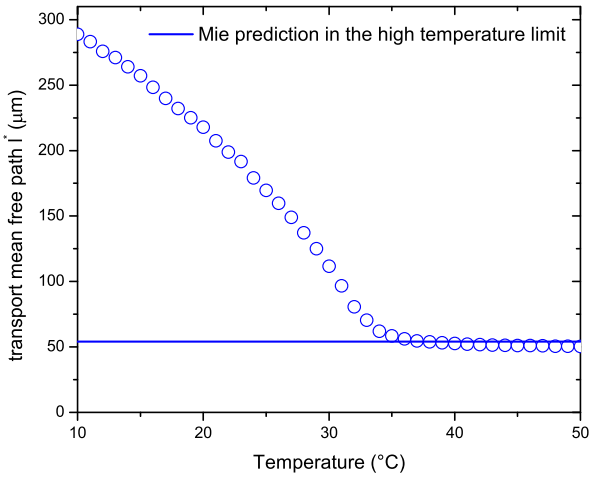

Fig. 4. Transport mean free path l^* as a function of temperature for a concentrated system (mass density approximately 14.6% w/w). Solid line: Mie result, $l^* = 56\,\mu\mathrm{m}$, for homogenous hard spheres with radius $R = 242\,\mathrm{nm}$ at an effective volume fraction of $\Phi \approx 19\%$.

Figure 4 shows the corresponding increase of the transport mean free path upon decreasing the temperature. The optical transport mean free path increases from $l^* = 53\,\mu\mathrm{m}$ in the high-temperature limit ($T = 40°$) to $l^* = 289\,\mu\mathrm{m}$ at $T = 10°$.

By lowering its density, the cross-linked gel changes its optical properties. In fact, the swollen gel has a lower optical contrast compared to the collapsed gel. Further scattering contrast is lost as particles start to touch and deform. For perfectly homogeneous particles at an effective volume fraction of 1 there should be no scattering. Residual scattering can be linked to density fluctuations that are due to: a) the imperfect space filling of the PNIPAM microgel particles; b) an inhomogeneous radial density distribution of the individual particles; c) positional correlations. In our case positional correlations contribute only weakly to the increase of l^* since the structure factor peak is located at small values of q compared to the cut-off value $2 \cdot k_0$.

At high temperatures the system is fluid, particles are homogenous and moreover the density is only moderately high. Under these conditions it should be possible to make a quantitative prediction of l^* using equation (6) [46,49]. For our analysis we use the radius obtained from static light scattering, $R = 242\,\mathrm{nm}$. Structural correlations are taken into account using the Perkus-Yevick structure factor for a monodisperse suspension of hard spheres. For pure water as a solvent ($n_s = 1.33$) and a particle index $n_s = 1.46$ we find a value of $l^* = 56\,\mu\mathrm{m}$ ($l^* = 48\,\mu\mathrm{m}$ with $S(q) \equiv 1$) at a suspension volume fraction of $\Phi = 19\%$. Such an exceptionally good agreement with the experimental result $l^* = 53\,\mu\mathrm{m}$ must be somewhat fortuitous

given the limited accuracy of our input parameters such as particle refractive index and the effective volume fraction.

Finally we would like to add a comment concerning the background medium refractive index. Previous studies on mono- and biomodal suspension of polystyrene spheres ($n \simeq 1.6$) up to $\Phi \simeq 40\%$ found good agreement between theory (Eq. (6)) and experiment using the refractive index of pure water [46,50]. For high-refractive-index particles ($n > 2$) at high volume fraction (in air) it is, however, necessary to take into account an increased effective refractive as shown by Gómez Rivas *et al.* [51] and more recently Reufer and co-workers [52]. Following the latter approach, in our case we obtain $n_{\text{solvent, eff}} \simeq 1.346$ and thus $l^* = 75\,\mu$m.

6 Summary and conclusions

In summary we have presented a comprehensive study of the scattering properties of a temperature tunable colloidal system. It would be interesting to further extend our approach by using additional techniques such as Ultra Small Angle X-Ray or Neutron Scattering to access information on smaller length scales as done in some of the previous work on similar systems. The particular system presented in this work displays some interesting properties which make it very suitable to study the phase behavior of colloids with repulsive interactions. The particles are charge stabilized in the maximally collapsed state and therefore fully stable even at high temperatures. The optical transport mean free path at $T = 40\,^\circ$C furthermore indicates that at high temperatures the system essentially behaves as a suspension of hard spheres. This in turn will allow the system to reversibly cross the phase boundary from a dense colloidal suspension to an arrested system upon changing the temperature.

Work supported by the TOP NANO 21 Initiative, Grant No. 5971.2, the Swiss National Science Foundation, projects No. 200020-117762 and No. 200020-117755, and the Marie Curie network Grant No. MRTN-CT2003-504712. Authors also thank Christoph Neururer and Daniela Curdy for SEM facility and synthesis assistance, Peter Schurtenberger, James Harden, Reinhard Sigel, Nasser Ben Braham, Veronique Trappe, Joaquim Clara Rahola, Frederic Cardinaux and Pavel Zakharov for discussions.

References

1. J. Wu, Z. Hu, in *Encyclopedia of Nanoscience and Nanotechnology* edited by J.A. Schwartz, C.I. Contescu, K. Putyera (Marcel Dekker Inc., 2004), pp. 1967-1976.
2. H. Senff, W. Richtering, J. Chem. Phys. **111**, 1705 (1999).
3. C. Wu, S. Zhou, Macromolecules **30**, 574 (1997).
4. J.D. Debord, S. Eustis, S.B. Debord *et al.*, Adv. Mater. **14**, 658 (2002).
5. L.F. Rojas-Ochoa, J.M. Mendez-Alcaraz, J.J. Sáenz, P. Schurtenberger, F. Scheffold, Phys. Rev. Lett. **93**, 073903 (2004).
6. A.M. Schmidt, Colloid Polym. Sci. **285**, 953 (2007).
7. M. Karg, I. Pastoriza-Santos, J. Perez-Juste, T. Hellweg, L.M. Liz-Marzan, Small **3**, 1222 (2007).
8. N. Dingenouts, Ch. Norhausen, M. Ballauff, Macromolecules **31**, 8912 (1998).
9. K. Otake, H. Inomata, M. Konno, S. Saito, Macromolecules **23**, 283 (1990).
10. X. Wu, R.H. Pelton, A.E. Hamielec *et al.*, Colloid Polym. Sci. **272**, 467 (1994).
11. M. Shibayama, Macromol. Chem. Phys. **199**, 1 (1998).
12. T. Hellweg, C.D. Dewhurst, E. Bruckner, K. Kratz, W. Eimer, Colloid Polym. Sci. **278**, 972 (2000).
13. T. Eckert, E. Bartsch, Phys. Rev. Lett. **89**, 125701 (2002).
14. P.N. Pusey, W. van Megen, Nature **320**, 340 (1986).
15. Ch. Beck, W. Härtl, R. Hempelmann, J. Chem. Phys. **111**, 8209 (1999).
16. J.J. Crassous, M. Siebenburger, M. Ballauff *et al.*, J. Chem. Phys. **125**, 204906 (2006).
17. A.N.S. John, V. Breedveld, L.A. Lyon, J. Phys. Chem. B **111**, 796 (2007).
18. L.A. Lyon, J.D. Debord, S.B. Debord *et al.*, J. Phys. Chem. B **108**, 19099 (2004).
19. J.Z. Wu, B. Zhou, Z.B. Hu, Phys. Rev. Lett. **90**, 048304 (2003).
20. K. Kratz, T. Hellweg, W. Eimer, Polymer **42**, 6631 (2000).
21. I. Deike, M. Ballauff, N. Willenbacher, A. Weiss, J. Rheol. **45**, 709 (2001).
22. P. Díaz-Leyva, M. Reufer, I. Lynch, J.L. Harden, F. Scheffold, submitted.
23. J.J. Crassous, M. Siebenburger, M. Ballauff, M. Drechsler, D. Hajnal, O. Henrich, M. Fuchs, J. Chem. Phys. **128**, 204902 (2008).
24. P.J. Flory, *Principles of Polymer Chemistry* (Cornell University Press, New York, 1953).
25. I. Varga, T. Gilanyi, R. Meszaros, G. Filipcsei, M. Zrinyi, J. Phys. Chem. B **105**, 9071 (2001).
26. M. Stieger, W. Richtering, J.A. Pedersen, P. Lindner, J. Chem. Phys. **120**, 6197 (2004).
27. T. Hellweg, C.D. Dewhurst, W. Eimer, K. Kratz, Langmuir **20**, 4330 (2004).
28. S. Seelenmeyer, I. Deike, S. Rosenfeldt, C. Norhausen, N. Dingenouts, M. Ballauff, T. Narayanan, P. Lindner, J. Chem. Phys. **114**, 10471 (2001).
29. A.K. Lele, M.M. Hirve, M.V. Badinger, R.A. Mashelkar, Macromolecules **30**, 157 (1997).
30. H.G. Schild, Progr. Polym. Sci. **17**, 163 (1992).
31. W. McPhee, K.C. Tam, R. Pelton, J. Colloid Interface Sci. **156**, 24 (1993).
32. A. Erbe, K. Tauer, R. Sigel, Phys. Rev. E **73**, 031406 (2006).
33. R.S. Chen, H. Yang, X.H. Yan, Z.L. Wang, L. Li, Chem. J. Chin. U. **22**, 1262 (2001).
34. J. Brandrup, E.H. Immergut, E.A. Grulke, A. Abe, D.R. Bloch (Editors), *Polymer Handbook*, 4th edition (John Wiley & Sons, 2005).
35. J.C. Maxwell-Garnett, Philos. Trans. R. Soc. London, Ser. A **203**, 385 (1904).
36. M. Born, E. Wolf, *Principles of Optics*, 3rd edition (Pergamon, Oxford, 1965).
37. B.J. Berne, R. Pecora, *Dynamic Light Scattering* (Wiley, New York, 1976).
38. P. Schurtenberger, M.E. Newman, in *Environmental Particles*, edited by J. Buffle, H.P. van Leeuwen (Lewis Publishers, Boca Raton, 1993), Chapt. 2, pp. 37-115.

39. C. Urban, P. Schurtenberger, J. Colloid Interface Sci. **207**, 150 (1998).
40. H.C. van de Hulst, *Light Scattering by Small Particles* (Dover, New York, 1981); C.F. Bohren, D.R. Huffman, *Absorption and Scattering of Light by Small Particles* (John Wiley & Sons, Inc., New York, 1983).
41. Polydisperse Mie data calculated using the MiePlot software (`http://www.philiplaven.com/mieplot.htm`).
42. A. Fernandez-Nieves, F.J. de las Nieves, A. Fernandez-Barbero, J. Chem. Phys. **120**, 374 (2004).
43. T.G. Mason, M.Y. Lin, Phys. Rev. E **71**, 040801 (2005).
44. A. Ishimaru, *Wave Propagation and Scattering in Random Media* (Academic Press, New York, 1978).
45. D.A. Weitz, D.J. Pine, *Dynamic Light Scattering*, edited by W. Brown (Oxford University Press, New York, 1993), Chapt. 16, pp. 652-720.
46. S. Fraden, G. Maret, Phys. Rev. Lett. **65**, 512 (1990).
47. P.D. Kaplan, M.H. Kao, A.G. Yodh, D.J. Pine, Appl. Opt. **32**, 3828 (1993).
48. B.R. Dasgupta, S.Y. Tee, J.C. Crocker, B.J. Frisken, D.A. Weitz, Phys. Rev. E **65**, 05505 (2002).
49. L.F. Rojas-Ochoa, S. Romer, F. Scheffold, P. Schurtenberger, Phys. Rev. E **65**, 051403 (2002).
50. P.D. Kaplan, A.G. Yodh, D.J. Pine, Phys. Rev. Lett. **68**, 393 (1992).
51. J. Gómez Rivas, D.H. Dau, A. Imhof, R. Sprik, B.P.J. Bret, P.M. Johnson, T.W. Hijmans, A. Lagendijk, Opt. Commun. **220**, 17 (2003).
52. M. Reufer, L.F. Rojas-Ochoa, S. Eiden, J.J. Sáenz, F. Scheffold, Appl. Phys. Lett. **91**, 171904 (2007).